

Structure of the zinc-bound amino-terminal domain of the NMDA receptor NR2B subunit

Erkan Karakas, Noriko Simorowski
and Hiro Furukawa*

WM Keck Structural Biology Laboratory, Cold Spring Harbor Laboratory,
Cold Spring Harbor, NY, USA

N-methyl-D-aspartate (NMDA) receptors belong to the family of ionotropic glutamate receptors (iGluRs) that mediate the majority of fast excitatory synaptic transmission in the mammalian brain. One of the hallmarks for the function of NMDA receptors is that their ion channel activity is allosterically regulated by binding of modulator compounds to the extracellular amino-terminal domain (ATD) distinct from the L-glutamate-binding domain. The molecular basis for the ATD-mediated allosteric regulation has been enigmatic because of a complete lack of structural information on NMDA receptor ATDs. Here, we report the crystal structures of ATD from the NR2B NMDA receptor subunit in the zinc-free and zinc-bound states. The structures reveal the overall clamshell-like architecture distinct from the non-NMDA receptor ATDs and molecular determinants for the zinc-binding site, ion-binding sites, and the architecture of the putative phenylethanolamine-binding site.

The EMBO Journal (2009) 28, 3910–3920. doi:10.1038/emboj.2009.338; Published online 12 November 2009

Subject Categories: neuroscience; structural biology

Keywords: allosteric inhibition; crystallography; NMDA receptor; zinc binding

Introduction

L-glutamate is the major excitatory neurotransmitter in the mammalian brain and is critically involved in brain development and function. Fast excitatory neurotransmission is mediated by release of L-glutamate from nerve terminals followed by activation of a class of ligand-gated ion channel called ionotropic glutamate receptors (iGluRs) in the post-synaptic membrane (Kandel *et al*, 1995). The iGluR family is divided into three subfamilies based on pharmacological sensitivity to the synthetic compounds, α -amino-3-hydroxy-5-methyl-4-isoxazole propionic acid, kainate, and N-methyl-D-aspartate (NMDA). Each subfamily comprises multiple genes encoding subunit proteins that assemble as tetrameric ion channels within the same group (Dingledine *et al*, 1999).

NMDA receptors are unique ligand-gated ion channels, which require multiple events for activation, including the binding of two agonists, L-glutamate and glycine, and the

relief of a Mg^{2+} block by membrane depolarization (Mayer *et al*, 1984; Johnson and Ascher, 1987). In agreement with the requirement of both glycine and L-glutamate for activation, NMDA receptors are heterotetrameric ion channels composed of two copies each of the obligatory glycine-binding NR1 subunit and the L-glutamate-binding NR2 and/or the glycine-binding NR3 subunits (Cull-Candy *et al*, 2001). The four distinct NR2 subunits (A–D) combine with the splice variants of the NR1 subunit to convey multiple subtypes with distinct ion channel properties and spatial and temporal expression patterns (Monyer *et al*, 1994). The opening of NMDA receptor ion channels results in influx of cations, including Ca^{2+} into the postsynapse and activates signal transduction cascades that control synaptic strength (MacDermott *et al*, 1986). This coincidental integration of chemical and electrical information into a Ca^{2+} signal is crucial for activity-dependent synaptic plasticity underlying neuronal development and memory formation (Kerchner and Nicoll, 2008; Sudhof and Malenka, 2008). In contrast, dysfunction of NMDA receptors is implicated in numerous neurological diseases and disorders, including seizure, stroke, Parkinson's disease, Alzheimer's disease, and schizophrenia (Cull-Candy *et al*, 2001).

The architecture of NMDA receptors, like the other subfamily members of iGluRs, is modular and is composed of multiple domains with distinct functional roles (Figure 1A) (Kuusinen *et al*, 1995). The large extracellular region of iGluRs is partitioned into two domains, an amino-terminal domain (ATD) and a ligand-binding domain (LBD) (S1S2). The S1S2 LBD binds glutamate and glycine and elicits opening of the ion channel pore formed by the transmembrane domains (TM) in the heterotetrameric assembly. In the S1S2 domain, NMDA receptors and non-NMDA receptors have rather high sequence similarity ($\sim 50\%$ similar) and similar overall architectures as revealed by recent crystallographic studies (Armstrong and Gouaux, 2000; Furukawa and Gouaux, 2003; Furukawa *et al*, 2005; Mayer, 2005; Yao *et al*, 2008). In contrast, ATDs of NMDA receptors and non-NMDA receptors have little or no sequence homology. Most importantly, although there is no ATD-targeted ligand or evidence for the ATD-mediated functional regulation in non-NMDA receptors, there is a rich spectrum of small ligands that bind the ATD of NMDA receptors and allosterically modulate ion channel activity (Paoletti and Neyton, 2007). These ligands are small molecules and ions including polyamines, phenylethanolamines, or Zn^{2+} that bind to ATD in a subunit-specific manner; that is, polyamines and protons bind NR1 (Traynelis *et al*, 1995; Masuko *et al*, 1999), Zn^{2+} binds both NR2A (Paoletti *et al*, 1997, 2000; Choi and Lipton, 1999; Fayyazuddin *et al*, 2000; Low *et al*, 2000) and NR2B (Rachline *et al*, 2005), and phenylethanolamine compounds bind NR2B (Perin-Dureau *et al*, 2002). In particular, zinc is found at many excitatory synapses in the brain and thus is likely to be a natural ligand of ATD (Paoletti *et al*, 2009).

From the clinical perspective, the ATD-mediated allosteric modulation of NMDA receptors has evoked considerable

*Corresponding author. WM Keck Structural Biology Laboratory, Cold Spring Harbor Laboratory, 1 Bungtown Road, Cold Spring Harbor, NY 11724, USA. Tel.: +1 516 367 8872; Fax: +1 516 367 8873; E-mail: furukawa@cshl.edu

Received: 5 September 2009; accepted: 21 October 2009; published online: 12 November 2009

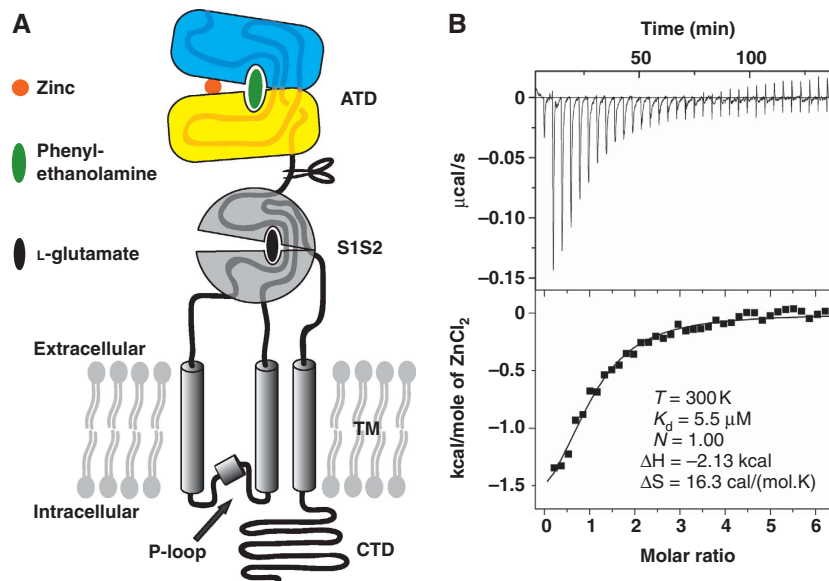


Figure 1 Isolated NR2B ATD proteins bind zinc. (A) Domain organization of the NR2B subunit. ATD in cyan (R1 domain) and yellow (R2 domain) binds allosteric modulators including zinc and phenylethanolamine, S1S2 binds neurotransmitter L-glutamate, the transmembrane domain (TM) and the P-loop (arrow) form the ion channel pore, and the C-terminal domain (CTD) binds postsynaptic molecules and mediates intracellular signalling. NR2B ATD can be isolated and recombinantly expressed in insect cells. (B) ITC analysis of zinc binding to the NR2B ATD protein. Upper panel, calorimetric titration of 0.8 mM ZnCl_2 into 0.02 mM NR2B ATD. Lower panel, integrated heat as a function of Zn^{2+} / protein molar ratio with experimental data (filled squares) and the best fit (solid line). The K_d of zinc binding is calculated to be 5.5 μM .

interest because the effect of allosteric modulator compounds is highly subtype specific (Gogas, 2006). In particular, the phenylethanolamine compounds that target NR2B ATD have high efficacy and specificity and show some promise as neuroprotective agents without adverse side effects usually observed with antagonists targeting the S1S2 LBDs (Gogas, 2006). However, despite a great deal of enthusiasm, knowledge about the mechanism of the ATD-mediated allosteric inhibition in NMDA receptors remains incomplete because of lack of structural information on the NMDA receptor ATD. Thus, to gain insight into the basic mechanisms underlying recognition of allosteric modulator compounds at the NMDA receptor ATD, we have obtained crystal structures of the NR2B ATD in the zinc-free and zinc-bound states. The structures reveal an overall clamshell-like architecture in the closed conformation that is robustly different from the ones observed in non-NMDA receptor ATDs (Clayton *et al*, 2009; Jin *et al*, 2009; Kumar *et al*, 2009), and pinpoint the molecular determinants for the zinc-binding site and the putative phenylethanolamine-binding site at the clamshell cleft.

Results and discussion

Function of NR2B ATD

The NR2B NMDA receptor subunit has a modular molecular organization like other members of the iGluR family (Figure 1A), which allows the ATD to be isolated and expressed recombinantly. Together with a signal peptide from human placental alkaline phosphatase, the rat NR2B ATD, defined as a peptide from Ser 31 to Met 394, can be expressed as a secreted protein in the insect cell/baculovirus system.

One of the hallmarks of NR2B-containing NMDA receptors is that the ATD binds both Zn^{2+} or phenylethanolamine and inhibits the ion channel activity in a non-competitive manner

(Perin-Dureau *et al*, 2002; Rachline *et al*, 2005). To examine whether the recombinantly expressed NR2B ATD proteins retain an ability to bind Zn^{2+} , we measured heat changes resulting from an incremental addition of Zn^{2+} to the purified NR2B ATD protein by isothermal titration calorimetry (Figure 1B). Fitting of the isotherm shows the presence of one Zn^{2+} -binding site per protein molecule with K_d of 5.5 μM , which is roughly comparable to the IC_{50} value for the Zn^{2+} -mediated allosteric inhibition of the NR1/NR2B NMDA receptor ion channel activity (Rachline *et al*, 2005). Similar NR2B ATD constructs expressed in *Escherichia coli* (Wong *et al*, 2005; Han *et al*, 2008) are reported to bind ifenprodil and related compounds as assessed by circular dichroism and radio ligand-binding assay. Thus, the NR2B ATD proteins studied here retain a functional characteristic of the intact NR1/NR2B NMDA receptors.

Structure determination

To reveal the atomic structure of an NMDA receptor ATD, we conducted a crystallographic study on NR2B ATD. The following manipulations were critical for obtaining a sufficient quantity of the NR2B ATD protein suitable for crystallographic studies: (1) use of an amino-terminal octa-histidine tag for purification with metal-chelating chromatography, (2) mutation of one of the three putative N-linked glycosylation sites, Asn348 to Asp, and (3) use of a baculovirus strain with deletion of viral genes, *V-cath* and *chiA* (Fitzgerald *et al*, 2006), together with the High Five cell-line. The combination of the above manipulations improved the expression level by five-fold and resulted in a yield of ~0.5 mg of the homogeneously purified NR2B ATD protein per litre of insect cell culture. Unlike non-NMDA receptors that form dimers in solution with K_d of ~150 nM (GluR2) and ~10 μM (GluR6), the NR2B ATD proteins are monomers at 5 mg/ml (~120 μM)

as analysed by sedimentation velocity using analytical ultracentrifugation (Supplementary Figure S1).

To understand the molecular mechanism underlying zinc recognition, the NR2B ATD proteins were crystallized in the presence and absence of Zn^{2+} . In both cases, the NR2B ATD proteins crystallized in space group $P3_121$ with similar unit cell dimensions and with one NR2B ATD protomer per asymmetric unit. Despite the unusually high solvent content of the crystals (77%), the *x*-ray diffraction limit of the zinc-bound and zinc-free crystal extended to 3.2 and 2.8 Å, respectively (Supplementary Table SI), which was sufficient to unambiguously model most of the amino-acid backbones and side chains starting from Pro 32 to Met 394 except for a disordered region between residues 208 and 214 (Figure 2; Supplementary Figure S2). The structure of the zinc-free form was solved by multiple isomorphous replacement with anomalous scattering (MIRAS) using single anomalous diffraction (SAD) datasets from crystals incorporated with Ta_6Br_{14} , $ErCl_3$, K_2AuBr_4 , and *L*-selenomethionine (SeMet) (Supplementary Table SI). The use of the above four heavy atoms for phasing was necessary to obtain an interpretable electron density map (Supplementary Figure S3). Subsequently, the structure of NR2B ATD in the zinc-bound state was obtained by molecular replacement using the zinc-free structure as a search probe. After iterative rounds of refinement, the final structures had acceptable conventional *R*-factor and *R*_{free} and stereochemical statistics (Supplementary Table SII).

Overall architecture of NR2B ATD

The NR2B ATD has an overall clamshell-like architecture composed of two domains, R1 and R2, which are tied

together by three well-structured loops (Figure 2). The crystals grown in the presence and absence of zinc both contain one NR2B ATD molecule per asymmetric unit. Consistent with the result from sedimentation velocity, there is no apparent evidence for a formation of physiological dimers. This is in contrast to GluR2 and GluR6 ATDs, which form dimers in solution as well as in crystals (Clayton *et al*, 2009; Jin *et al*, 2009; Kumar *et al*, 2009). The packing pattern of the NR2B ATD protomers in the $P3_121$ crystal does not share any common feature observed in GluR2 ATD or GluR6 ATD.

The NR2B ATD contains two types of posttranslational modifications, *N*-linked glycosylation and a disulfide bond. Clear electron density for *N*-acetyl-glucosamine is present at the two *N*-linked glycosylations sites, Asn 74 and Asn 341, both of which are located within the R1 domain. The first ordered residue, Pro 32, is at the ‘top’ of R1, whereas the last residue of the protein construct, Met 394, is at the ‘bottom’ of R2. Thus, our NR2B ATD structure suggests that the beginning of the S1S2 LBD in the NMDA receptor subunits is located at the ‘bottom’ portion of the R2 domain far away from the *N*-terminus. The architecture of the R1 domain is further organized by the presence of a disulfide bond formed between two conserved cysteine residues, Cys 86 from Helix 1 and Cys 321 from a ‘hypervariable loop’ (HVL; Figure 2). Similar disulfide bonds are also observed in GluR2 and GluR6 ATDs. Thus, the disulfide bond formation between Helix 1 and HVL is most likely a conserved feature of all iGluR ATDs. The HVL (L1 ‘flap’ and Loop 3 in GluR2 and GluR6, respectively) is formed by the 15–20 amino-acid long linker between Helix 8 and 9 in NR2B whose primary sequence is conserved within each subfamily but is highly variable between the three subfamilies (Supplementary Figure S2). In GluR2 and GluR6 ATDs, HVLs

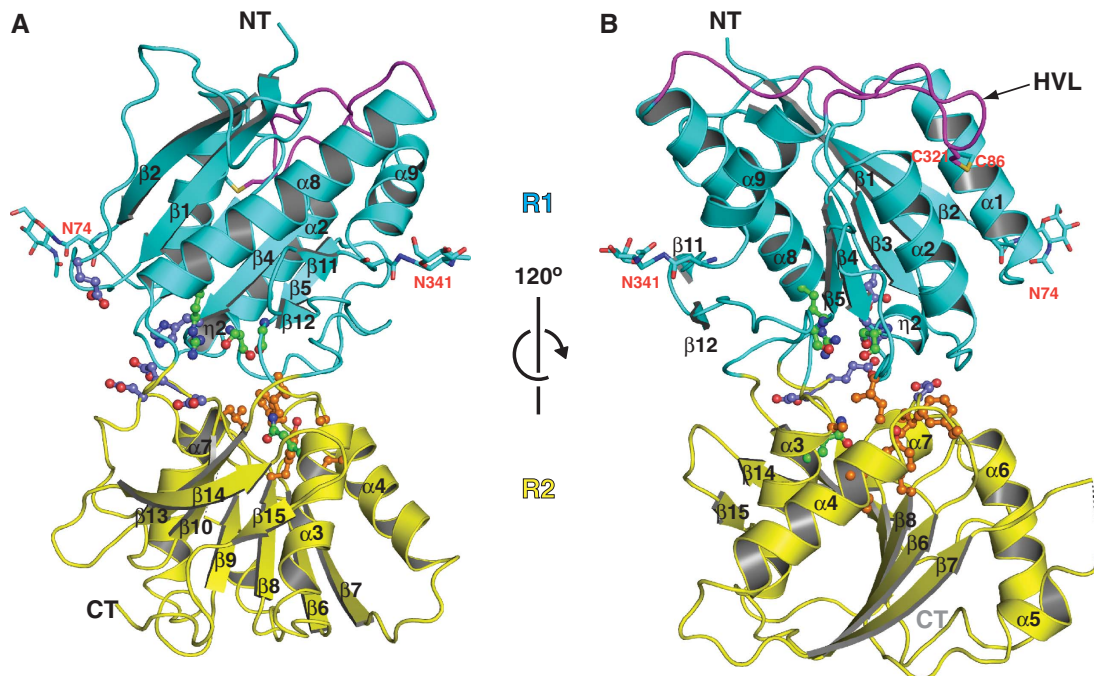


Figure 2 Overall architecture of NR2B ATD. (A) Ribbon representation of the NR2B ATD structure in complex with zinc. The clamshell-like architecture of NR2B ATD is composed of two domains, R1 (cyan) and R2 (yellow), defined as residues 32–147 and 287–359 and residues 148–286 and 360–394, respectively. Hypervariable loop (HVL; in magenta) is oriented by a disulfide bond so that it covers the ‘top’ of the R1 domain. The disordered region (residues 208–214) between $\beta 7$ and $\alpha 5$ is indicated with a dashed line. Stick representations are used to show the disulfide bond (Cys 86–Cys 321), and sugar molecules attached to Asn 74 and Asn 341. Residues involved in zinc inhibition, phenylethanolamine inhibition, and ion binding are represented by balls and sticks in blue, orange, and green, respectively. (B) View of the NR2B ATD structure from the ‘entrance’ of the clamshell.

protrude towards the homodimer interface, thus, they have been suggested to have a function in a subtype-specific assembly of iGluRs (Clayton *et al*, 2009; Jin *et al*, 2009; Kumar *et al*, 2009). Because of the structural conservation around the region, it is plausible that HVL also has a function in subunit assembly in NMDA receptors.

The cleft of the NR2B ATD clamshell can be partitioned into three different regions based on their chemical properties and functional roles (Figure 2). First, the ‘hydrophilic pocket,’ which contains a cluster of polar residues including His 127 and Glu 284 involved in zinc binding (blue sticks). Second, the ‘hydrophobic pocket’ at the inner core of the clamshell, which contains a cluster of hydrophobic residues including Ile 133, Ile 150, Phe 176, Tyr 231, and Leu 261 critical for ifenprodil sensitivity (orange sticks). And third, the ‘ion-binding site’ located in between the ‘hydrophilic’ and ‘hydrophobic’ pockets, which contains residues including Ser 131, Phe 146, and Gln 153 and accommodates Na and Cl ions (green sticks). In both zinc-bound and zinc-free structures, Na and Cl ions are present at this ion-binding site.

Distinct architecture of NR2B ATD from non-NMDA receptor ATDs

The overall fold of NR2B ATD has an approximate similarity to non-NMDA receptor GluR2 ATD (Clayton *et al*, 2009; Jin *et al*, 2009) or GluR6 ATD (Kumar *et al*, 2009), but, with a significantly distinct conformation. The root-mean-square deviation of the entire ATD is high with values of 4.3 Å over 276 C α positions and 3.6 Å over 245 C α positions between NR2B and GluR2 and NR2B and GluR6, respectively. However, when the R1 and R2 domains are individually superimposed, the root-mean-square deviation values are significantly lower: 2.4 Å over 158 C α positions (R1) and 2.2 Å over 145 C α positions (R2) between NR2B ATD and GluR2 ATD and 2.2 Å over 152 C α positions (R1) and 1.9 Å over 142 C α positions (R2) between NR2B ATD and GluR6 ATD (Figure 3A). This major difference is caused by the distinct R1–R2 domain orientation, which in NR2B ATD, is ‘twisted’ by a striking rotation of ~ 45 and 54° compared with the R1–R2 orientation in GluR2 ATD or GluR6 ATD (Figure 3C).

What could be a potential cause for this ‘twisted’ conformation in NR2B ATD? The structural overlay shows a lack of ~ 30 residues between β -strand 10 and Helix 8 in NR2B ATD compared with non-NMDA receptors (Figure 3A and C; Supplementary Figure S2). These 30 residues in non-NMDA receptors form a motif with an α helix that couples R1 and R2 (Jin *et al*, 2009; Kumar *et al*, 2009) and potentially stabilizes the closed conformation of GluR2 and GluR6 ATD clamshell. Thus, it is plausible that the lack of the helical motif in NR2B ATD provides a structural freedom to orient the R1 and R2 domains in the ‘twisted’ conformation. The absence of this structural motif is a general feature of all of the NMDA receptor subunits, and therefore we suggest that the ‘twisted’ conformation observed in the current NR2B ATD structure is a unique aspect of NMDA receptor ATD structures. Furthermore, it is important to point out that this large structural difference prevents the NR2B ATD protomers to form a homo dimer in a similar protomer arrangement to that observed in GluR2 or GluR6 ATD. For example, when two copies of the NR2B ATD protomers are superimposed onto the GluR6 ATD dimer at R1, most of the R2 residues from the two protomers clash against each other (Supplementary

Figure S4). Thus, we suggest that the dimeric arrangement of NMDA receptor ATDs is substantially different from that of non-NMDA receptor ATDs.

The NR2B ATD also has distinct surface properties from non-NMDA receptor ATDs. Of note is the presence of the large hydrophobic patch at the ‘bottom’ of the R2 domain that is only present in NR2B ATD (Figure 4). We propose that the large hydrophobic patch may be a region that has a function in inter-domain and/or inter-subunit interactions, which is crucial for the ATD-mediated allosteric regulation. Overall, the distinct structural features of NR2B ATD compared with non-NMDA receptor ATDs described above may be critical in eliciting the ATD-mediated regulation of the ion channel activities, which is observed only in NMDA receptors but not in non-NMDA receptors.

Structural comparison of NR2B ATD with mGluR LBD

The NR2B ATD structure also has a similar overall fold to the LBDs of metabotropic glutamate receptors (mGluRs) and atrial natriuretic peptide (ANP) receptors, and bacterial leucine/isoleucine/valine-binding protein (LIVBP) as predicted earlier by O’Hara *et al* (1993) although sequence identity of the aligned region is only 11–16%. The most homologous structure is the LBD of mGluR1 (PDB code: 1EWK) (Kunishima *et al*, 2000), with a root-mean-square deviation of 3.4 Å but over only 251 out of 365 possible C α positions. When the structures of the R1 and R2 domains are individually superimposed to the mGluR1 LBD structure, the root-mean-square deviation is significantly lower with 2.4 Å for R1 and 2.0 Å for R2 over 150 and 143 C α positions, respectively (Figure 3B). This difference in the root-mean-square deviation values, as in the case of the structural difference between NR2B ATD and non-NMDA receptor ATDs, is due to the ‘twisted’ R1–R2 orientation of NR2B ATD (Figure 3D). The R1–R2 orientation of GluR2 and GluR6 ATDs is similar to that of mGluR LBDs, ANP receptor LBDs, and LIVBP. Thus, the ‘twisted’ conformation of NR2B ATD is unique among the iGluRs and other families of receptors derived from LIVBP.

Zinc binds to NR2B ATD clamshell cleft

To reveal the molecular determinant for a zinc-binding site in NR2B ATD, we solved the structure in complex with ZnCl₂. The crystallographic analysis of NR2B ATD shows that the molecular determinants for the zinc-binding site are distinct from those proposed for the hydrophobic pocket that is implicated in phenylethanolamine sensitivity. Five zinc-binding sites (Zn1–5) within the NR2B ATD protomer are unambiguously identified by calculating the anomalous difference Fourier map (Figure 5A). No anomalous peak is observed when difference Fourier map at the zinc peak wavelength (1.28 Å) is calculated from data for zinc-free crystals, indicating that zinc does not remain bound during protein purification and that the zinc anomalous peak observed in the zinc-bound NR2B ATD structure is derived from zinc added to the crystallization solution. Among the five zinc sites identified, Zn2, Zn3, and Zn5 are on the protein surface, whereas Zn4 is at the crystallographic contact that is likely to be non-physiological and Zn1 is at the inter-domain cleft of the NR2B ATD clamshell containing residues implicated in zinc sensitivity. Although binding of zinc ions to the Zn2, 3, and 5 sites in the physiological condition cannot be ruled out, there seems to be no functional role

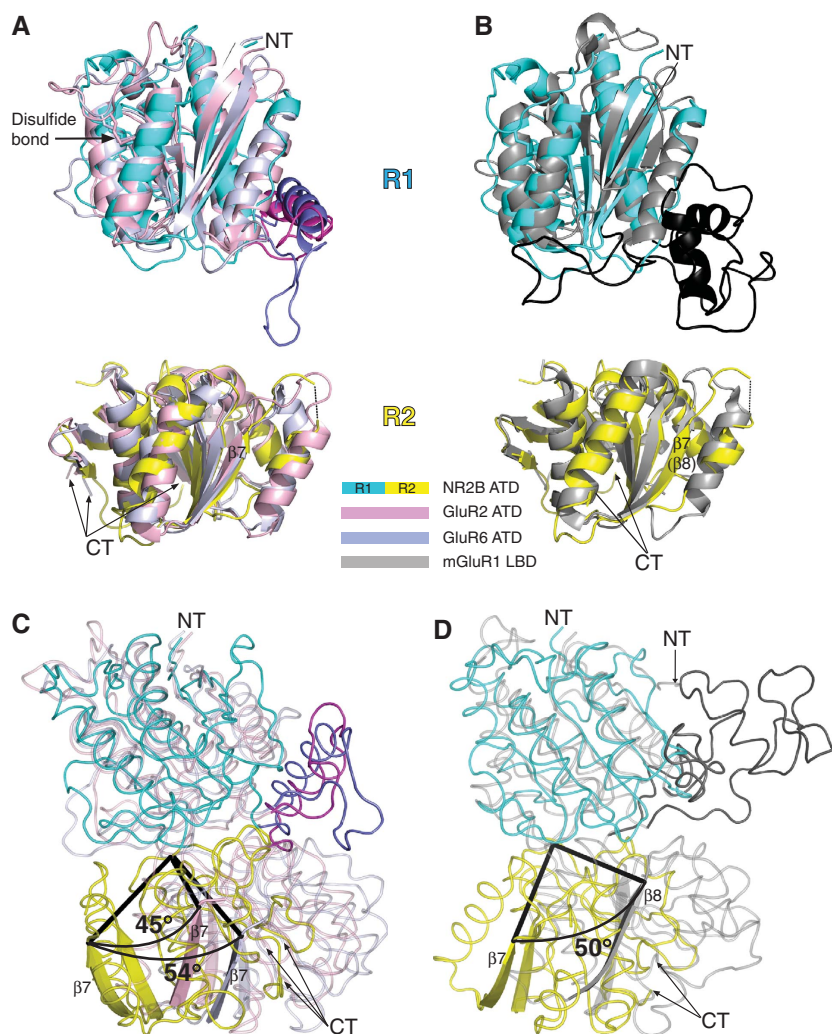


Figure 3 NR2B ATD has a different bi-lobe orientation from non-NMDA receptor ATD or mGluR1 LBD. (A) Superposition of the R1 (cyan, upper panel) and R2 (yellow, lower panel) domains of NR2B ATD with the equivalent domains of GluR2 ATD (pink, PDB code: 3H5V, chain A) and GluR6 ATD (light blue, PDB code: 3H6G, chain B). The regions of GluR2 ATD (Helix 8) and GluR6 ATD (Helix L), which are absent in NR2B ATD, are highlighted in magenta and blue, respectively. Disulfide bonds are shown in sticks (arrow). The root-mean-square deviations are 2.37 Å (R1, 152 C α s) and 2.17 Å (R2, 142 C α s) and 2.18 Å (R1, 152 C α s) and 1.85 Å (R2, 142 C α s) for GluR2 and GluR6 ATDs, respectively. (B) Superposition of NR2B ATD domains with the equivalent domains of mGluR1 LBD (grey, PDB code: 1EWK, chain A). The regions of mGluR1 LBD, which are absent in NR2B ATD, are coloured in black. The root-mean-square deviations are 2.4 Å (R1, 150 C α s) and 2.0 Å (R2, 143 C α s). (C) Superposition of the R1 domains from GluR2 and GluR6 ATDs onto the R1 domain of NR2B ATD illustrates a large difference in the pattern of the R1–R2 inter-domain orientation. The R2 domain of NR2B ATD is rotated by $\sim 45^\circ$ and $\sim 54^\circ$ relative to the R2 domains of GluR2 and GluR6 ATDs, respectively. The reference rods (in black) for the angle measurement are drawn from the pivotal point of the rotation (NR2B Pro 148, GluR2 Asp 131 and GluR6 Asp 152) to the last residue of $\beta 7$ in all three structures. (D) The same manipulation as in (C) illustrates the ‘twisted’ R1–R2 inter-domain orientation of NR2B ATD compared with mGluR1 LBD by $\sim 50^\circ$. The two reference rods for the angle measurements in mGluR1 LBD are drawn from Pro 206 to the end of $\beta 8$.

for these zinc ions because mutations of residues His 359, His 60, and His 311 to alanine, at the respective sites, do not cause any major change in zinc sensitivity as assessed by dose-response analyses by two electrode voltage-clamp (TEVC) (Supplementary Table SIII). Consistent with this, earlier electrophysiological studies have suggested the presence of one zinc-binding site in NR2A ATD and NR2B ATD owing to the observation that the zinc dose-response curves fit well with single-binding site isotherms with a Hill coefficient value of ~ 1 (Paoletti *et al*, 1997; Rachline *et al*, 2005). Thus, for the above reasons, we attribute Zn1 to be the zinc-binding site responsible for the voltage-independent zinc inhibition.

Zn1 is situated at the ‘hydrophilic pocket’ at the outer end of the R1–R2 inter-domain cleft and is in close proximity to

the polar residues Glu 47, Asp 102, His 127, Asp 265, Asp 283, and Glu 284. Binding of Zn1 involves direct contact of His 127 from R1 and Glu 284 from R2, which stabilizes the closed clamshell conformation. Although involvement of His 127 has been shown earlier (Rachline *et al*, 2005), the critical function of Glu 284 was not predicted from the mGluR1 LBD-based homology model (Marinelli *et al*, 2007) because of a large difference between the model and the current crystal structure derived from the unexpected $\sim 50^\circ$ twist between R1 and R2 as described above. Other polar residues including Glu 47 and Asp 265 face the Zn1 site, however, with no direct contact with Zn1; the distances between the side chains of Glu 47 and Asp 265 and Zn1 are 6.1 and 6.3 Å, respectively. Mutations of both Glu 47 and Asp 265 to alanine have been shown earlier to reduce zinc sensitivity by four-fold (Rachline

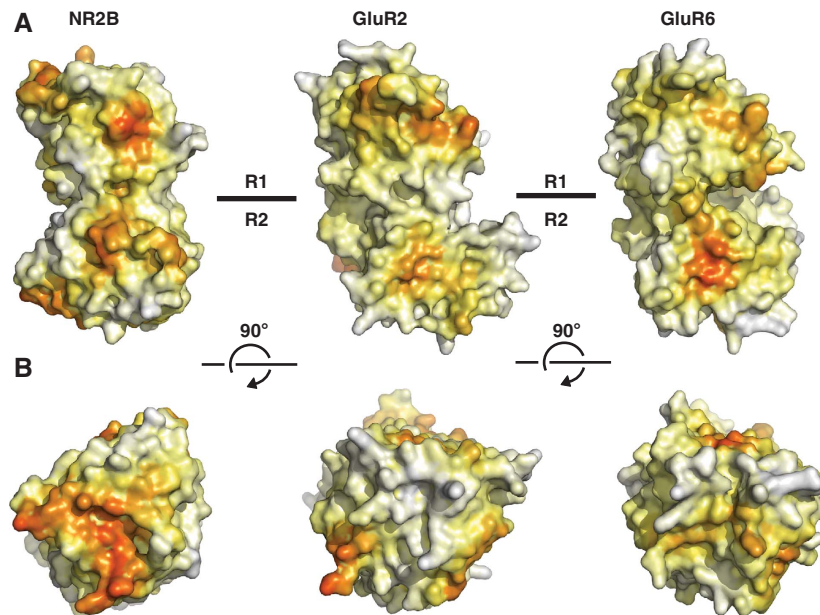


Figure 4 Surface presentation of NR2B ATD and non-NMDA receptor ATDs. Surface presentation is coloured by hydrophobicity. **(A)** The R1 domains of NR2B, GluR2, and GluR6 ATDs are superimposed and viewed onto the dimer interface from the same angle. GluR6 ATD has a notable hydrophobic patch composed of five hydrophobic residues in R2, whereas NR2B ATD has a smaller hydrophobic patch formed by Tyr 175, Tyr 179, and Leu 204. **(B)** The surface presentation viewed from the 'bottom' of the R2 domain. Unlike non-NMDA receptor ATDs, NR2B ATD contains a large hydrophobic patch composed of Tyr 164, Trp 166, Ile 168, Phe 194, Val 195, Pro 226, Ile 227, Tyr 389, Val 390, and Trp 391. Hydrophobicity was calculated using the hotpatch server (<http://hotpatch.mbi.ucla.edu/>). The surface was coloured from hydrophobic to hydrophilic in a dark orange to white gradient.

et al, 2005). Thus, although we cannot assign water molecules at the current resolution (3.2 Å), it is plausible that the function of Glu 47 and Asp 265 may be to facilitate binding of Zn1 indirectly by placing water molecules at the coordination position through hydrogen bonds. Asp 101, Asp 102, and Thr 103 are on the loop that extends from β 3 and towards the Zn1 site (Figure 5B). Among those residues, Asp 102 is facing the Zn1 site but is distant from the zinc ion (>6 Å). Consistently, the Asp102Ala mutation has been shown earlier to have no effect on zinc sensitivity (Rachline *et al*, 2005). In contrast, Asp 101 and Thr 103 are the residues that affect both ifenprodil and zinc sensitivities when mutated to alanine (Rachline *et al*, 2005). In the current crystal structure, both Asp 101 and Thr 103 face the opposite direction to Zn1 and form a hydrogen bond network with the main chain nitrogens of Gly 129 and Ser 130 (Figure 5B). Thus, Asp 101 and Thr 103 are critical residues required to maintain the architecture of the Zn1 pocket and the NR2B ATD clamshell structure as a whole.

To test the physiological relevance of the current crystal structure, we have mutated newly identified residues around the Zn1 site, including Asp 283 and Glu 284, to alanine and quantified zinc inhibition by measuring IC_{50} using TEVC. Consistent with the current crystal structures, removal of the zinc coordinating carboxylate groups by the Glu284Ala mutation causes approximately a five-fold increase in the IC_{50} value (Figure 5C; Supplementary Table SIII). In contrast, an alanine mutation of Asp 283, a residue that does not participate in the coordination of Zn1, only shows minor effect. The His127Ala/Asp283Ala/Glu284Ala mutant has a similar degree of change in IC_{50} , indicating that disruption of either His 127 or Glu 284 is sufficient to hamper the coordination of Zn1. In all of the cases above, the mutants are only able to shift the IC_{50} values to 5–6 μ M. A similar effect has been

observed for the analysis of the high-affinity zinc inhibition site in NR2A where mutations of the binding residues were only able to shift the IC_{50} values to the low micromolar range (Fayyazuddin *et al*, 2000). This is most likely attributed to the presence of the low-affinity Zn^{2+} inhibitory site conserved across the NR2 subtypes as suggested earlier by Neyton and colleagues (Fayyazuddin *et al*, 2000).

Furthermore, mutation of all of the above residues has little or no effect on ifenprodil sensitivity indicating that the residues involved in Zn1 binding are distinct from those involved in ifenprodil binding (Figure 5D). Earlier work has shown that binding of zinc and ifenprodil compete with each other (Rachline *et al*, 2005). Although a structural mechanism cannot be established at present because of the lack of an NR2B ATD structure in the ifenprodil-bound form, one possible explanation for the observation is that zinc blocks ifenprodil from binding to the NR2B ATD clamshell by keeping the clamshell conformation closed. Taken together, the current crystal structure and electrophysiological data clearly shows the direct involvement of His 127 and Glu 284 and indirect involvement of Glu 47 and Asp 265 in the coordination of Zn1.

The NR2A-containing NMDA receptors are also allosterically inhibited by extracellular zinc (Paoletti *et al*, 1997) but with much higher sensitivity than NR2B-containing NMDA receptors; IC_{50} values of zinc inhibition are 16 and 760 nM for NR2A and NR2B, respectively (Rachline *et al*, 2005). As the ATDs of NR2A and NR2B are 56% identical, we predict that the architecture around the Zn1 site is similar. Therefore, the current structure of NR2B ATD along with an amino-acid sequence alignment allows us to propose a potential mechanism underlying the difference in zinc sensitivity between the two subunits. The most notable difference between NR2A and NR2B is on the loop that extends from β strand 1 and

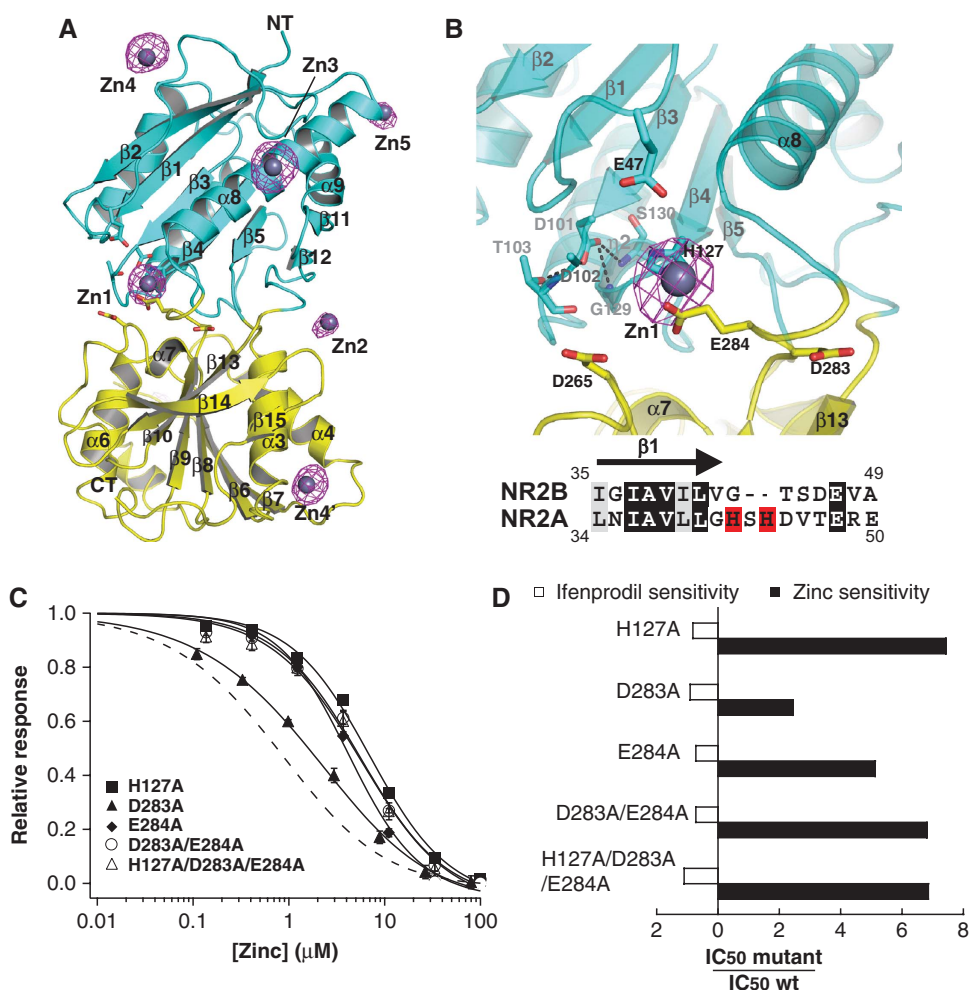


Figure 5 Zinc-binding site. (A) Crystal structure of NR2B ATD in complex with zinc coloured as cyan (R1) and yellow (R2). The mesh in magenta represents the zinc anomalous difference map contoured at 6.0σ . There are five zinc molecules identified per asymmetric unit (Zn1–5). Zn4 and Zn4' are related by crystallographic symmetry. (B) Zoom up view of the Zn1 site. Zn1 is directly coordinated by the His 127 and Glu 284 side chains. Residues including Glu 47 and Asp 265 are too far from Zn1 ($> 5 \text{ \AA}$) to make direct contacts but may be involved in placing water molecules around Zn1 through hydrogen bonds. Side chain of Asp 102 beyond β carbon is disordered in the zinc-bound structure. (C) Mutagenesis and the zinc dose–response curve showing an involvement of His 127 and Glu 284 in zinc sensitivity. Mutation of residues directly involved in the Zn1 coordination (His 127 and Glu 284) has significant effect on zinc sensitivity, whereas that of non-contacting residue, Asp 283, has minor effect. All of the recordings were done at the holding potential of -40 mV . The wild-type response is shown by a dotted line. The error bars represent standard deviation for recordings from at least four different oocytes. (D) Fold difference in zinc and ifenprodil sensitivities in each mutant. Mutation of the Zn1 site residues (His 127 and Glu 284) has a major effect on zinc sensitivity but little or no effect on ifenprodil sensitivity.

contains Glu 47 (Figure 5B). The equivalent region of NR2A has additional two amino-acid residues and contains two histidine residues, His 42 and His 44, which are critically involved in zinc sensitivity (Fayyazuddin *et al*, 2000). Consequently, His 42 and His 44 may be able to position themselves in close proximity to Zn1 and form more ideal coordination along with His 128 (His 127 in NR2B), and Asp 283 (Glu 284 in NR2B). Although the architecture of the zinc-binding site between NR2A and NR2B may be distinct from each other, we propose that a difference in the number of direct coordination (four for NR2A and two for NR2B) may be one of the factors underlying the large difference in zinc sensitivity between the two subunits.

NR2B ATD in zinc-free form

The structure of NR2B ATD in a zinc-free form also captured the closed cleft conformation in the current crystallographic study (Figure 6A). Except for the Zn1-binding site where

there is a major structural rearrangement, the overall conformation of NR2B ATD in the zinc-free and zinc-bound forms are similar to each other with a root-mean-square deviation of 0.56 \AA over 356 $\text{C}\alpha$ positions (Supplementary Figure S5). This observation is in contrast to LIVBP, which undergoes a robust $\sim 50^\circ$ clamshell closure on binding of amino-acid ligands (Trakhanov *et al*, 2005) or to the mGluR1 LBD that also experiences significant clamshell closure on binding of L-glutamate (Kunishima *et al*, 2000). Careful inspection of the crystal structures in both the zinc-bound and zinc-free forms reveals the presence of electron density that represents one Na ion and three Cl ions deep in the middle of the clamshell cleft between the zinc-binding site and the hydrophobic pocket (Figure 6A and B). The presence of Na and Cl ions are further confirmed by calculating anomalous difference Fourier maps using data collected on rubidium and bromide soaked crystals, respectively (Figure 6C and D). Rubidium, in general, binds better to sites, which

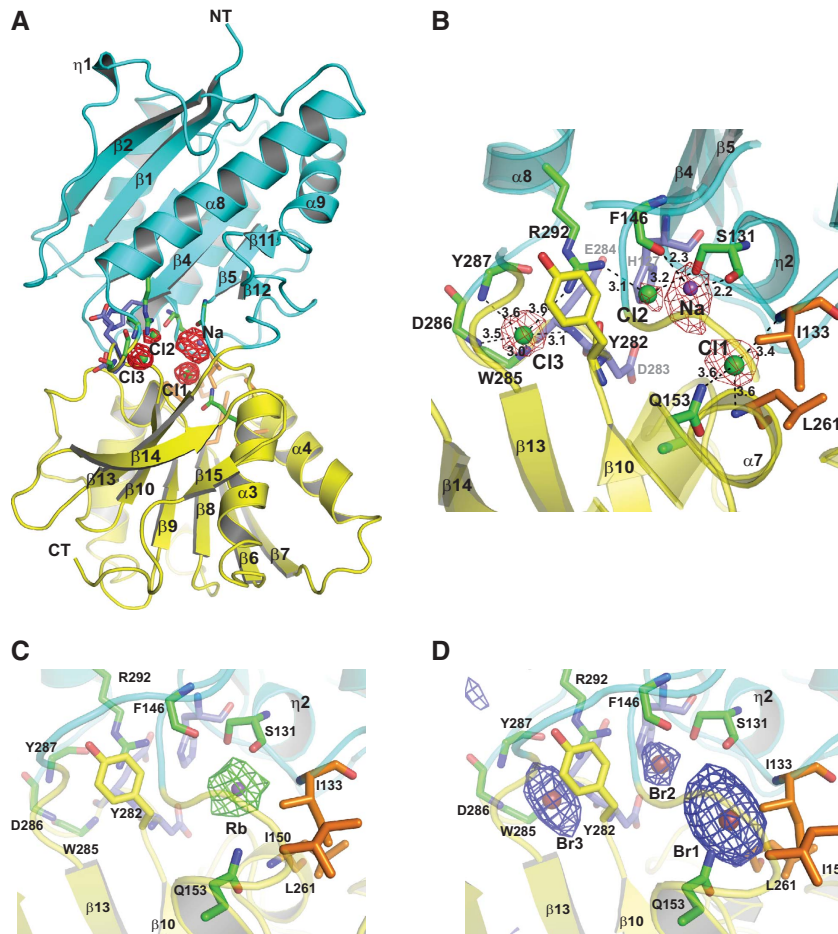


Figure 6 Structure of NR2B ATD in the zinc-free form. (A) The crystal structure of NR2B ATD in the absence of zinc at 2.8 Å. The structure is coloured as in Figure 2. The red mesh represents $F_o - F_c$ omit map at 5.0 σ for one Na ion and three chloride ions (Cl1–3) at the clamshell cleft. (B) The zoom up view of the ion-binding site at the clamshell cleft. Na and Cl ions are coloured as purple and green, respectively. Residues involved in ion binding, zinc binding, and phenylethanolamine binding are coloured in green, blue, and orange, respectively. (C) Anomalous difference map at 3.3 σ calculated from data collected on Rb soaked crystals showing that the density has an overlap with the Na-binding site. (D) Anomalous difference map at 4.2 σ calculated from data collected on Br soaked crystals showing that Br can substitute all of the Cl sites at the cleft.

are selective for potassium. However, in the current structure, it is able to replace the Na ion-binding site at the identical position indicating that the cation-binding site is not highly specific for Na ion. This observation is in parallel with Na ion binding in the LBD of GluR6 where Na ions can be substituted with other monovalent cations, including Li^+ , K^+ , Rb^+ , and Cs^+ (Plested *et al*, 2008). Binding of the Na and Cl ions involves residues from both R1 and R2 domains (Figure 6B). Cl1 is located proximal to the hydrophobic pocket and coordinated by main chain nitrogens of Ile 133, Leu 261, and side chain of Gln 153, whereas Cl2 is proximal to the zinc-binding site and is coordinated by side chains of Ser 131 and Arg 292. Cl3 is located at the back side of the Zn1 site, which involve the main chain nitrogens of Trp 285, Asp 286, and Tyr 287 and the side chain of Arg 292 (Figure 6B). The Na ion is located in between Cl1 and Cl2 and is coordinated by main chain oxygen of Ser 131 and Phe 146 with the coordination distance of 2.2 and 2.3 Å, respectively (Figure 6B). These values are within an appropriate range of the mean carbonyl- Na^+ and carboxylate- Na^+ distance observed in the Protein data bank (2.42 Å) (Harding, 2002). Sodium ions are most commonly coordinated by six ligands (Harding, 2002), thus, we anticipate that several water

molecules are also involved in the Na^+ coordination even though they are not clearly visible in the current structure because of insufficient resolution. Can physiological concentration of Na^+ and Cl^- induce clamshell closure? To date, there has not been any known mechanism for a functional modulation of NMDA receptors by monovalent ions such as Na^+ and Cl^- like the ones observed in kainate receptors (Plested and Mayer, 2007; Plested *et al*, 2008). Indeed, we have not observed any significant change in the current-voltage relationship by substitutions of Na^+ by Li^+ or Rb^+ or Cs^+ and Cl^- by NO_3^- at 150 mM salt concentration (data not shown). Thus, although binding of Na^+ and Cl^- can take place at the NR2B ATD clamshell cleft, it is likely not a driving force for the clamshell closure.

It has recently been suggested that the NR2B ATD clamshell can go through spontaneous oscillation between the open-cleft and closed-cleft conformations favouring channel opening and closing, respectively, and that binding of modulators including zinc and phenylethanolamine shifts the conformational equilibrium of ATD to the closed-cleft (Gielen *et al*, 2009). One of the hallmarks of the NR2B NMDA receptors is its low ion channel open probability and it has been shown that ATD is critically involved in this process (Gielen *et al*, 2009). This implies that

NR2B ATD is favoured to be in the closed conformation even in the absence of zinc and phenylethanolamine. Thus, it is plausible that the current crystallographic study on the zinc-free form may have simply captured the closed conformation—a more favourable conformation than the open conformation in NR2B.

Residues at the R1–R2 interface have a significant function in controlling the activity of NMDA receptors containing NR2B. One notable residue is, Tyr282, a residue from R2 located deep in the middle of the clamshell cleft (Figure 6B). Mutating Tyr 282 to cysteine and modifying it with methane thiosulfonate (MTS) derivatives has been shown to dramatically increase the open probability by locking the clamshell open (Gielen *et al*, 2009). Furthermore, the alanine mutation of Arg 292 from R2, which forms an inter-domain hydrogen bond with the main chain oxygen of Tyr 282 and indirect inter-domain interactions through C12 and C13, lowers potency for zinc and ifenprodil inhibitions (Supplementary Table SIII). On the basis of our current crystal structure, it seems possible that the MTS modification of Tyr 282 or the Arg292Ala mutation perturbs the architecture around the clamshell cleft and destabilizes the closed conformation, thereby shifting the conformational equilibrium of ATD to the open-cleft form and favouring the opening of the ion channels or the lowering potency of allosteric inhibition. Taken together, the cleft residues at and around the ion-binding site are important structural motif that controls the opening and closing of the NR2B ATD clamshell and the ion channel activity.

Hydrophobic pocket

The NR2B ATD clamshell contains a hydrophobic pocket at the inner core of the cleft, which is formed by a cluster of hydrophobic residues including Ile 133, Ile 150, Phe 176, Phe 182, Tyr 231, and Leu 261 (Figures 2, 6 and 7 in orange sticks). Among these residues, mutations of the residues from the R2 domain including Ile 150, Phe 176, Phe 182, Tyr 231, and Leu 261 to alanine have been shown earlier to reduce ifenprodil sensitivity significantly (Perin-Dureau *et al*, 2002; Alarcon *et al*, 2008; Mony *et al*, 2009). Ile 133 is a residue from the R1 domain, which extends towards the core of the hydrophobic pocket. Indeed the side chain of Ile 133 is in van der Waals contact with Ile 150, Phe 176, Tyr 231, and Leu 261. To test whether this newly identified residue in the hydro-

phobic pocket, Ile 133, is involved in ifenprodil sensitivity, we have mutated Ile 133 to alanine and serine and tested for an ifenprodil dose–response using TEVC. Consistent with the crystal structure, the Ile133Ala or Ile133Ser mutation has a significant effect on ifenprodil sensitivity (Figure 7B). For both Ile133Ala and Ile133Ser, data points can be fitted to two-site model, but not one-site model Hill equation. It has been shown earlier that the NR2B subunit contains two ifenprodil-binding sites: a voltage-independent high-affinity site at ATD and voltage-dependent low-affinity site at the ion channel pore (Williams, 1993; Perin-Dureau *et al*, 2002). Thus, the high- and low-affinity components in the Ile 133 mutants likely represent the ATD-mediated inhibition and the ion channel block present at -20 mV holding potential, respectively (Figure 7B). The efficacy of the ATD-mediated ifenprodil inhibition is 40% of the peak current in these mutants, whereas the efficacy is $\sim 90\%$ in wild type. Of interest to note is the two modes of ifenprodil binding suggested recently by homology modelling of NR2B ATD and docking of ifenprodil (Mony *et al*, 2009). One possible explanation for the half reduction of the ATD-mediated inhibition is that the mutation may have hampered one of the two binding modes. Furthermore, consistent with the crystal structure, mutations of residues distant from the core of the hydrophobic pocket including Pro148Gly, Pro148Ser, and Tyr356Ala, have little or no effect on ifenprodil sensitivity (Figure 7B; Supplementary Table SIII). Taken together, the hydrophobic pocket in the NR2B ATD cleft is a key locus for ifenprodil sensitivity and contains residues from both the R1 and R2 domains. Unfortunately, despite extensive crystallization trials, we have not been able to obtain the structure of the NR2B ATD-ifenprodil complex.

Conclusion

This study provides the first molecular view of an NMDA receptor ATD. The novel ‘twisted’ conformation of the NR2B ATD maps previously unpredicted residues in the zinc-binding site and the putative phenylethanolamine-binding site. Together with structure-based mutagenesis and electrophysiology, the study provides a molecular insight into the recognition of zinc and elements that contribute to inhibition by phenylethanolamines. Furthermore, this study has identified sodium- and chloride-binding sites at the clamshell cleft,

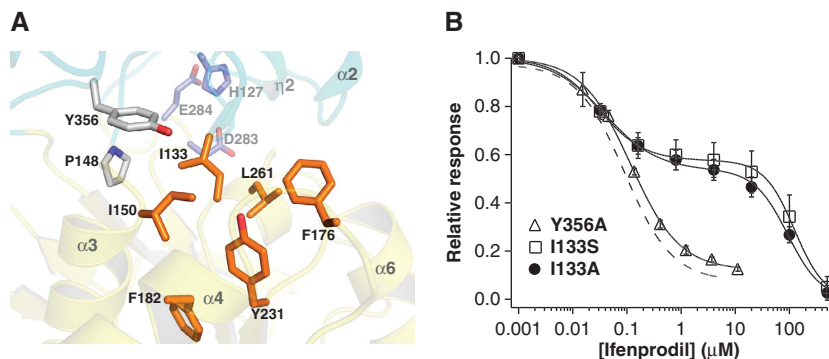


Figure 7 Hydrophobic pocket is the critical structural locus for ifenprodil sensitivity. (A) Hydrophobic residues responsible for ifenprodil sensitivity are clustered at the inner core of the NR2B ATD clamshell (in orange). Residues that have been mutated but had only minor effect are coloured in grey. (B) Dose response of ifenprodil showing the critical involvement of Ile 133 in ifenprodil inhibition. Mutation of Ile 133 to alanine or serine causes dramatic shift in ifenprodil sensitivity, whereas mutation of Tyr 356 to alanine has only minor effect. Data points for both wild type and Tyr356Ala are fit to a single-site model, whereas those for the Ile 133 mutants are fit to a two-site model described in ‘Materials and methods.’ The IC_{50} values calculated by the fits are listed in Supplementary Table SIII. The wild-type response is shown as a dotted line. All the currents were measured at the holding potential of -20 mV to minimize voltage-dependent pore block by ifenprodil.

the function of which remains to be established. The structural information obtained in this study may be applicable to understand the function of other NMDA receptor subunits.

Materials and methods

Expression, purification, and crystallization of NR2B ATD

The ATD of the rat NR2B (Ser 31 to Met 394) containing the Asn348Asp mutation was N-terminally fused to human placental alkaline phosphatase signal peptide followed by an octa-histidine tag and a thrombin cleavage site. The NR2B ATD proteins were expressed as secreted proteins using the High Five (*Trichoplusia ni*)/baculovirus system (DH10multibac) (Fitzgerald *et al*, 2006). The High Five cell culture (1.5×10^6 cells/ml) grown in ESF921 medium (Expression System) was infected with the recombinant virus harbouring NR2B ATD at multiplicity of infection of 5. After 48 h, the cell culture medium was collected, concentrated, and dialysed against 200 mM NaCl and 20 mM Tris-HCl (pH 8.0) using tangential flow filtration (Pall Corporation). NR2B ATD protein was purified by metal chelate chromatography, cleaved by thrombin to remove the N-terminal octa-histidine tag, and further purified by size-exclusion chromatography.

To produce SeMet-incorporated NR2B ATD protein, the culture medium was substituted with methionine-free ESF921 media 24 h after viral infection. After 4 h, DL-SeMet (Sigma) at 50 mg/l was added to the culture and the media was harvested 72 h after infection. The proteins were purified as described above in the presence of 2.5 mM methionine in all buffers to minimize oxidation of the SeMet residues.

Both the native and the SeMet incorporated NR2B ATD proteins were crystallized by hanging-drop vapour diffusion at 30°C by mixing the protein (8 mg/ml) with a reservoir solution containing 3.1–3.5 M NaCl, 2% PEG 400, 0.1 M MgCl₂, and 0.1 M acetate (pH 5.5) in 2:1 ratio. Crystals were cryoprotected in 4.6 M NaCl, 2% PEG400, and 0.1 M acetate (pH 5.5). Heavy atom derivatives for phasing were obtained by soaking native crystals in the cryosolutions supplemented with 0.2 mM Ta₆Br₁₆, 0.2 mM K₂AuBr₄, or 1 mM ErCl₃ for 1–5 h.

The NR2B ATD-zinc co-crystals were grown in a similar condition but in the presence of 0.1 mM ZnCl₂. The crystals were further soaked against a solution containing 3 M NaCl, 1 mM ZnCl₂, and 0.1 M MES (pH 6.0) for 2 h and cryoprotected in 4.7 M NaCl, 1 mM ZnCl₂, and 0.05 M MES (pH 6.0). To obtain bromide and rubidium derivatives, the zinc-free NR2B ATD crystals were soaked against 2 M Li₂SO₄, 1 M NaBr, and 0.1 M acetate (pH 5.5) for 2 h or 2 M RbCl and 1 M Mg-acetate (pH 5.0) for 1 min, respectively, and crystals were flash frozen in the soaking solutions.

Data collection and structural analysis

All x-ray diffraction data were collected at the X25 and X29 beamlines at National Synchrotron Light Source and processed using HKL2000 (Otwinowski and Minor, 1997). Diffraction data for heavy atom derivatives was collected at their respective peak wavelengths (Supplementary Table S1). Initially, three Ta₆Br₁₆ cluster sites were found by an SAD experiment at 6 Å resolution using SOLVE (Terwilliger, 2004). The phase information from the Ta₆Br₁₆ sites was used to calculate sites for Er, Au, and SeMet. MIRAS was done using the program SHARP (de La Fortelle and Bricogne, 1997). At this stage, a readily interpretable electron density map was obtained (Supplementary Figure S3). A poly-alanine model was built for 296 out of 365 residues using the

program RESOLVE. The rest of the model was built manually using O (Jones and Kjeldgaard, 1997) and COOT (Emsley and Cowtan, 2004). Structural refinement was performed using the program PHENIX (Adams *et al*, 2002) and REFMAC (Murshudov *et al*, 1997).

The structure of the zinc derivative was solved by molecular replacement using coordinates of the R1 and R2 domains of NR2B ATD as search probes and by conducting a multi-domain search in the program PHASER (McCoy *et al*, 2007). Prime and Switch phasing was carried out to remove model bias using the program RESOLVE (Terwilliger, 2004). The zinc atoms were unambiguously identified based on the anomalous difference Fourier map.

Isothermal titration calorimetry

NR2B ATD protein purified as above was extensively dialysed against a buffer containing 20 mM Tris-HCl (pH 7.4) and 150 mM NaCl and concentrated to ~20 μM. Calorimetric titrations were conducted on VP-ITC (MicroCal) and by successive injections of the zinc titrant (0.8 mM ZnCl₂) in 5 μl increments for 40 times at 27°C. Data analysis was done using the software ORIGIN 7.0 (OriginLab).

Electrophysiology

Recombinant NR1/NR2B NMDA receptors were expressed by co-injecting 0.1 ng of the rat NR1-1a and NR2B cRNAs at a 1:2 ratio (w/w) into defolliculated *Xenopus laevis* oocytes. The two-electrode voltage-clamp recordings were performed using agarose-tipped microelectrodes (0.4–1.0 MΩ) filled with 3 M KCl at a holding potential of –40 and –20 mV for zinc dose–response and ifenprodil dose–response analysis, respectively. The bath solution contained 5 mM HEPES, 100 mM NaCl, and 0.3 mM BaCl₂ at pH 7.3 (adjusted with KOH). Peak currents were measured by adding 100 μM each of the agonists, glycine and L-glutamate, and NR2B ATD-mediated inhibition was monitored in the presence of agonists and various concentrations of ifenprodil or ZnCl₂. For all of the zinc containing buffers, pH was readjusted. The data were acquired and analysed by the program Pulse (HEKA). Dose–response curves were plotted and fit using the program IgorPro (Wavemetrics).

Supplementary data

Supplementary data are available at *The EMBO Journal* Online (<http://www.embojournal.org>).

Acknowledgements

We thank staff from X25 and X29A at National Synchrotron Light Source for assistance in the collection of diffraction data. Ming Wang is thanked for maintenance of the home x-ray source. DH10multibac was a kind gift from Imre Berger. We thank Hermann Schindelin and Daniel P Raleigh for kindly sharing the ITC and AUC instrumentation. We also thank Mark Mayer, Lonnie Wollmuth, Iehab Talukder, and Leemor Joshua-Tor for critical reading of this manuscript. The coordinates and the structure factors are deposited to the Protein Data Bank with accession codes 3JPW and 3JPY for the zinc-free and zinc-bound NR2B ATD structures, respectively. This work was supported by Margaret and Richard Lipmanson Foundation, American Heart Association, Cold Spring Harbor Laboratory, and a donation from the McGuffog Family (HF). EK is a Harvey L Karp Fellow.

Conflict of interest

The authors declare that they have no conflict of interest.

References

- Adams PD, Grosse-Kunstleve RW, Hung LW, Ioerger TR, McCoy AJ, Moriarty NW, Read RJ, Sacchettini JC, Sauter NK, Terwilliger TC (2002) PHENIX: building new software for automated crystallographic structure determination. *Acta Crystallogr D Biol Crystallogr* **58**: 1948–1954
- Alarcon K, Martz A, Mony L, Neyton J, Paoletti P, Goeldner M, Foucaud B (2008) Reactive derivatives for affinity labeling in the ifenprodil site of NMDA receptors. *Bioorg Med Chem Lett* **18**: 2765–2770
- Armstrong N, Gouaux E (2000) Mechanisms for activation and antagonism of an AMPA-sensitive glutamate receptor: crystal structures of the GluR2 ligand binding core. *Neuron* **28**: 165–181
- Choi YB, Lipton SA (1999) Identification and mechanism of action of two histidine residues underlying high-affinity Zn²⁺ inhibition of the NMDA receptor. *Neuron* **23**: 171–180
- Clayton A, Siebold C, Gilbert RJ, Sutton GC, Harlos K, McIlhinney RA, Jones EY, Aricescu AR (2009) Crystal structure of the GluR2 amino-terminal domain provides insights into the architecture

- and assembly of ionotropic glutamate receptors. *J Mol Biol* **392**: 1125–1132
- Cull-Candy S, Brickley S, Farrant M (2001) NMDA receptor subunits: diversity, development and disease. *Curr Opin Neurobiol* **11**: 327–335
- de La Fortelle E, Bricogne G (1997) Maximum-likelihood heavy-atom parameter refinement for multiple isomorphous replacement and multiwavelength anomalous diffraction methods. *Methods Enzymol* **276**: 472–492
- Dingledine R, Borges K, Bowie D, Traynelis SF (1999) The glutamate receptor ion channels. *Pharmacol Rev* **51**: 7–61
- Emsley P, Cowtan K (2004) Coot: model-building tools for molecular graphics. *Acta Crystallogr D Biol Crystallogr* **60**: 2126–2132
- Fayyazuddin A, Villarreal A, Le Goff A, Lerma J, Neyton J (2000) Four residues of the extracellular N-terminal domain of the NR2A subunit control high-affinity Zn²⁺ binding to NMDA receptors. *Neuron* **25**: 683–694
- Fitzgerald DJ, Berger P, Schaffitzel C, Yamada K, Richmond TJ, Berger I (2006) Protein complex expression by using multigene baculoviral vectors. *Nat Methods* **3**: 1021–1032
- Furukawa H, Gouaux E (2003) Mechanisms of activation, inhibition and specificity: crystal structures of the NMDA receptor NR1 ligand-binding core. *EMBO J* **22**: 2873–2885
- Furukawa H, Singh SK, Mancusso R, Gouaux E (2005) Subunit arrangement and function in NMDA receptors. *Nature* **438**: 185–192
- Gielen M, Siegler Retchless B, Mony L, Johnson JW, Paoletti P (2009) Mechanism of differential control of NMDA receptor activity by NR2 subunits. *Nature* **459**: 703–707
- Gogas KR (2006) Glutamate-based therapeutic approaches: NR2B receptor antagonists. *Curr Opin Pharmacol* **6**: 68–74
- Han X, Tomitori H, Mizuno S, Higashi K, Full C, Fukuiwake T, Terui Y, Leewanich P, Nishimura K, Toida T, Williams K, Kashiwagi K, Igarashi K (2008) Binding of spermine and ifenprodil to a purified, soluble regulatory domain of the N-methyl-D-aspartate receptor. *J Neurochem* **107**: 1566–1577
- Harding MM (2002) Metal-ligand geometry relevant to proteins and in proteins: sodium and potassium. *Acta Crystallogr D Biol Crystallogr* **58**: 872–874
- Jin R, Singh SK, Gu S, Furukawa H, Sobolevsky AI, Zhou J, Jin Y, Gouaux E (2009) Crystal structure and association behaviour of the GluR2 amino-terminal domain. *EMBO J* **28**: 1812–1823
- Johnson JW, Ascher P (1987) Glycine potentiates the NMDA response in cultured mouse brain neurons. *Nature* **325**: 529–531
- Jones TA, Kjeldgaard M (1997) Electron-density map interpretation. *Methods Enzymol* **277**: 173–208
- Kandel ER, Schwartz JH, Jessell TM (1995) *Essentials of Neural Science and Behavior*. East Norwalk: Appelton & Lange
- Kerchner GA, Nicoll RA (2008) Silent synapses and the emergence of a postsynaptic mechanism for LTP. *Nat Rev Neurosci* **9**: 813–825
- Kumar J, Schuck P, Jin R, Mayer ML (2009) The N-terminal domain of GluR6-subtype glutamate receptor ion channels. *Nat Struct Mol Biol* **16**: 631–638
- Kunishima N, Shimada Y, Tsuji Y, Sato T, Yamamoto M, Kumasaka T, Nakanishi S, Jingami H, Morikawa K (2000) Structural basis of glutamate recognition by a dimeric metabotropic glutamate receptor. *Nature* **407**: 971–977
- Kuusinen A, Arvola M, Keinanen K (1995) Molecular dissection of the agonist binding site of an AMPA receptor. *EMBO J* **14**: 6327–6332
- Low CM, Zheng F, Lyuboslavsky P, Traynelis SF (2000) Molecular determinants of coordinated proton and zinc inhibition of N-methyl-D-aspartate NR1/NR2A receptors. *Proc Natl Acad Sci USA* **97**: 11062–11067
- MacDermott AB, Mayer ML, Westbrook GL, Smith SJ, Barker JL (1986) NMDA-receptor activation increases cytoplasmic calcium concentration in cultured spinal cord neurones. *Nature* **321**: 519–522
- Marinelli L, Cosconati S, Steinbrecher T, Limongelli V, Bertamino A, Novellino E, Case DA (2007) Homology modeling of NR2B modulatory domain of NMDA receptor and analysis of ifenprodil binding. *Chem Med Chem* **2**: 1498–1510
- Masuko T, Kashiwagi K, Kuno T, Nguyen ND, Pakh AJ, Fukuchi J, Igarashi K, Williams K (1999) A regulatory domain (R1–R2) in the amino terminus of the N-methyl-D-aspartate receptor: effects of spermine, protons, and ifenprodil, and structural similarity to bacterial leucine/isoleucine/valine binding protein. *Mol Pharmacol* **55**: 957–969
- Mayer ML (2005) Crystal structures of the GluR5 and GluR6 ligand binding cores: molecular mechanisms underlying kainate receptor selectivity. *Neuron* **45**: 539–552
- Mayer ML, Westbrook GL, Guthrie PB (1984) Voltage-dependent block by Mg²⁺ of NMDA responses in spinal cord neurones. *Nature* **309**: 261–263
- McCoy AJ, Grosse-Kunstleve RW, Adams PD, Winn MD, Storoni LC, Read RJ (2007) Phaser crystallographic software. *J Appl Cryst* **40**: 658–674
- Mony L, Krzaczkowski L, Leonetti M, Le Goff A, Alarcon K, Neyton J, Bertrand HO, Acher F, Paoletti P (2009) Structural basis of NR2B-selective antagonist recognition by N-methyl-D-aspartate receptors. *Mol Pharmacol* **75**: 60–74
- Monyer H, Burnashev N, Laurie DJ, Sakmann B, Seeburg PH (1994) Developmental and regional expression in the rat brain and functional properties of four NMDA receptors. *Neuron* **12**: 529–540
- Murshudov GN, Vagin AA, Dodson EJ (1997) Refinement of macromolecular structures by the maximum-likelihood method. *Acta Crystallogr D Biol Crystallogr* **53**: 240–255
- O'Hara PJ, Sheppard PO, Thogersen H, Venezia D, Haldeman BA, McGrane V, Houamed KM, Thomsen C, Gilbert TL, Mulvihill ER (1993) The ligand-binding domain in metabotropic glutamate receptors is related to bacterial periplasmic binding proteins. *Neuron* **11**: 41–52
- Otwinowski Z, Minor W (1997) Processing of X-ray diffraction data collected in oscillation mode. *Methods Enzymol* **276**: 307–326
- Paoletti P, Ascher P, Neyton J (1997) High-affinity zinc inhibition of NMDA NR1–NR2A receptors. *J Neurosci* **17**: 5711–5725
- Paoletti P, Neyton J (2007) NMDA receptor subunits: function and pharmacology. *Curr Opin Pharmacol* **7**: 39–47
- Paoletti P, Perin-Dureau F, Fayyazuddin A, Le Goff A, Callebaut I, Neyton J (2000) Molecular organization of a zinc binding N-terminal modulatory domain in a NMDA receptor subunit. *Neuron* **28**: 911–925
- Paoletti P, Vergnano AM, Barbour B, Casado M (2009) Zinc at glutamatergic synapses. *Neuroscience* **158**: 126–136
- Perin-Dureau F, Rachline J, Neyton J, Paoletti P (2002) Mapping the binding site of the neuroprotectant ifenprodil on NMDA receptors. *J Neurosci* **22**: 5955–5965
- Plested AJ, Mayer ML (2007) Structure and mechanism of kainate receptor modulation by anions. *Neuron* **53**: 829–841
- Plested AJ, Vijayan R, Biggin PC, Mayer ML (2008) Molecular basis of kainate receptor modulation by sodium. *Neuron* **58**: 720–735
- Rachline J, Perin-Dureau F, Le Goff A, Neyton J, Paoletti P (2005) The micromolar zinc-binding domain on the NMDA receptor subunit NR2B. *J Neurosci* **25**: 308–317
- Sudhof TC, Malenka RC (2008) Understanding synapses: past, present, and future. *Neuron* **60**: 469–476
- Terwilliger T (2004) SOLVE and RESOLVE: automated structure solution, density modification and model building. *J Synchrotron Radiat* **11**: 49–52
- Trakhanov S, Vyas NK, Luecke H, Kristensen DM, Ma J, Quiocho FA (2005) Ligand-free and -bound structures of the binding protein (LivJ) of the Escherichia coli ABC leucine/isoleucine/valine transport system: trajectory and dynamics of the interdomain rotation and ligand specificity. *Biochemistry* **44**: 6597–6608
- Traynelis SF, Hartley M, Heinemann SF (1995) Control of proton sensitivity of the NMDA receptor by RNA splicing and polyamines. *Science* **268**: 873–876
- Williams K (1993) Ifenprodil discriminates subtypes of the N-methyl-D-aspartate receptor: selectivity and mechanisms at recombinant heteromeric receptors. *Mol Pharmacol* **44**: 851–859
- Wong E, Ng FM, Yu CY, Lim P, Lim LH, Traynelis SF, Low CM (2005) Expression and characterization of soluble amino-terminal domain of NR2B subunit of N-methyl-D-aspartate receptor. *Protein Sci* **14**: 2275–2283
- Yao Y, Harrison CB, Freddolino PL, Schulten K, Mayer ML (2008) Molecular mechanism of ligand recognition by NR3 subtype glutamate receptors. *EMBO J* **27**: 2158–2170